Inorg. Chem. **2008**, *47*, 11212−11222

Structural Chemistry and Magnetic Properties of $Nd_{18}Li_8Fe_5O_{39}$ and $Nd_{18}Li_8Co_4O_{39}$: the Interplay of Cation and Spin Ordering

Siân E. Dutton,[†] Peter D. Battle,*[,†] Fernande Grandjean,[‡] Gary J. Long,*[,§] and Katsuyoshi Oh-ishi[||]

Inorganic Chemistry Laboratory, Department of Chemistry, University of Oxford, South Parks Road, Oxford OX1 3QR, U.K., Department of Physics, University of Liège, B5, B-4000 Sart-Tilman, Belgium, Department of Chemistry, Missouri University of Science and Technology, University of Missouri—Rolla, Rolla, Missouri 65409-0010, and Department of Applied Chemistry, Faculty of Science and Engineering, Chuo University, 1-13-27 Kasuga Bunkyo-ku Tokyo 112-8551 Japan

Received August 11, 2008

Polycrystalline samples of $Nd_{18}Li_8Fe_5O_{39}$ and $Nd_{18}Li_8Co_4O_{39}$ have been synthesized using a solid-state method and studied by a combination of neutron diffraction, direct and alternating current magnetometry, and, in the case of $Nd_{18}Li_8Fe_5O_{39}$, Mössbauer spectroscopy. Both compounds adopt a cubic structure (space group $Pm\bar{3}n$, $a_0 \sim 11.9$ Å) based on intersecting ⟨111⟩ chains made up of alternating octahedral and trigonal-prismatic coordination sites. The Fe^{4+} cations in $Nd_{18}Li_8Fe_5O_{39}$ are found on only the smaller of the two distinct octahedral sites in the structure; Fe^{3+} and Li^+ are disordered over the larger octahedral site and the trigonal-prismatic site. The Nd^{3+} cations occupy sites between the chains. The smaller octahedral site is fully occupied by cobalt in $Nd_{18}Li_8Co_4O_{39}$, with 25% of the larger octahedral sites being vacant; Li^+ is only found on the prismatic sites. $Nd_{18}Li_8Fe_5O_{39}$ shows spin-glass-like behavior with a spin-freezing temperature of 5.75 K, whereas $Nd_{18}Li_8Co_4O_{39}$ appears to order antiferromagnetically at 2.3 K. In both cases, the magnetic coupling involves the Nd^{3+} sublattice.

Introduction

Mixed-metal oxides with the general formula $A_3A'BO_6$ have played an integral part in recent research into the electronic properties of pseudo-one-dimensional materials.[1] These compounds are isostructural with rhombohedral K_4CdCl_6;[2] that is, $A'O_6$ trigonal prisms alternate with BO_6 octahedra to form polyhedral chains parallel to the 3-fold axis, with the A cations occupying the interchain space; neighboring polyhedra share a common triangular face. The structure is illustrated in Figure 1.

A range of magnetic properties has been observed in these materials. Sr_3LiRuO_6, in which the prismatic sites are occupied by diamagnetic Li^+ cations, orders as a collinear antiferromagnet upon cooling below 90 K.[3] This is an unusually high Néel temperature for an oxide containing the cation Ru^{5+} $4d^3$ from the second transition series and is made more remarkable by the relatively long superexchange pathways involved in both the intra- and interchain magnetic interactions. In other compositions, for example, $Ca_3Co_2O_6$,[4−6] Ca_3NiMnO_6,[7,8] and $Sr_3A'IrO_6$ ($A' = Ni, Cu$),[9] both of the six-coordinate sites are occupied by a 3d, 4d, or 5d transition-metal cation. The presence of magnetic cations on both sites can lead to complex behavior with the Néel temperature of a magnetically concentrated composition often being lower than that of magnetically dilute Sr_3LiRuO_6. Ca_3NiMnO_6, for example, adopts a spiral magnetic structure

* To whom correspondence should be addressed. E-mail: Peter.Battle@chem.ox.ac.uk (P.D.B.), glong@mst.edu (G.J.L.).
[†] University of Oxford.
[‡] University of Liège.
[§] University of Missouri—Rolla.
[||] Chuo University.

(1) Stitzer, K. E.; Darriet, J.; zur Loye, H.-C. *Curr. Opin. Solid State Mater. Sci.* **2001**, *5*, 535.
(2) Bergerhoff, G.; Schmitz-Dumont, O. *Naturwissenschaften* **1954**, *12*, 280.
(3) Darriet, J.; Grasset, F.; Battle, P. D. *Mater. Res. Bull.* **1997**, *32*, 139.
(4) Aasland, S.; Fjellvåg, H.; Hauback, B. *Solid State Commun.* **1997**, *101*, 187.
(5) Fjellvåg, H.; Gulbrandsen, E.; Aasland, S.; Olsen, A.; Hauback, B. C. *J. Solid State Chem.* **1996**, *124*, 190.
(6) Kageyama, H.; Yoshimura, K.; Kosuge, K.; Mitamura, H.; Goto, T. *J. Phys. Soc. Jpn.* **1997**, *66*, 1607.
(7) Bazuev, G. V.; Zubkov, V. G.; Berger, I. F.; Arbuzova, T. I. *Solid State Sci.* **1999**, *1*, 365.
(8) Kawasaki, S.; Takano, M.; Inami, T. *J. Solid State Chem.* **1999**, *145*, 302.
(9) Nguyen, T. N.; zur Loye, H.-C. *J. Solid State Chem.* **1995**, *117*, 300.

10.1021/ic801529m CCC: $40.75
Published on Web 10/29/2008

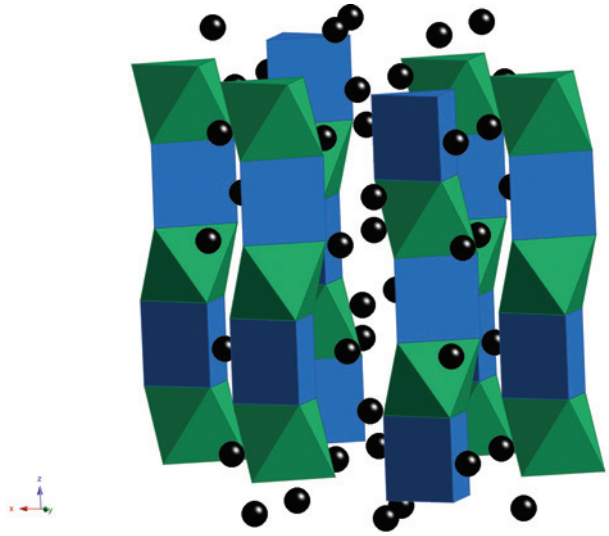

Figure 1. Sr_3LiRuO_6 phase in the K_4CdCl_6 structure. Black circles represent the Sr site and green octahedra the RuO_6 groups; the LiO_6 trigonal prism is blue.

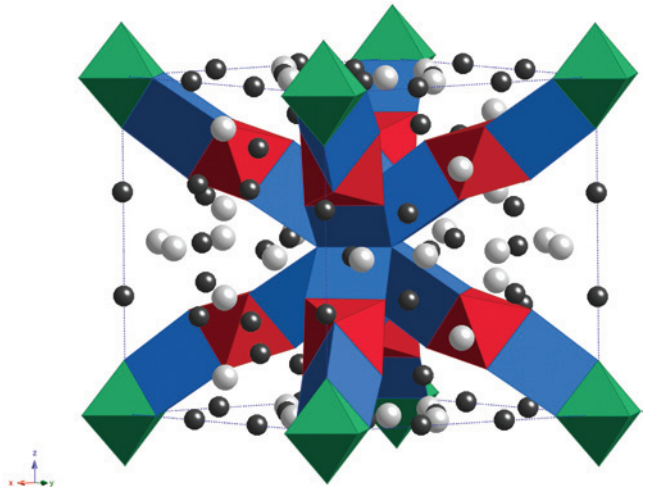

Figure 2. Cubic $Ln_{18}Li_8Rh_5O_{39}$ structure (space group $Pm\bar{3}n$). Gray circles represent oxygen and black circles lanthanide. The LiO_6 trigonal prisms are blue, and the RhO_6 octahedra are green (2*a* site) and red (8*e*). An additional 2*a* site is located at the center of the unit cell.

below a Néel temperature of 19 K, and $Ca_3Co_{1.04}Mn_{0.96}O_6$ has recently been described as a magnetoelectric material.[10]

The members of the $A_3A'BO_6$ family are not the only compounds to contain chains of alternating octahedral and prismatic coordination polyhedra. The same structural building block has been observed in cubic $Ln_{18}Li_8Rh_5O_{39}$ (Ln = La, Pr), with lithium and rhodium occupying the trigonal-prismatic and octahedral sites, respectively.[11] In this case, the polyhedral chains, which occupy tunnels within a Ln−O framework, run along the ⟨111⟩ directions of the unit cell and intersect each other at (0, 0, 0) and ($^1/_2$, $^1/_2$, $^1/_2$), as shown in Figure 2. Equivalent octahedral sites are located at these two points of intersection, and a further, crystallographically distinct octahedral site is located halfway between them; the two distinct types of octahedral sites are always separated from each other by a prismatic site. Analysis of neutron diffraction data showed that the octahedral sites at the points of intersection are significantly smaller than those at ($^1/_4$, $^1/_4$, $^1/_4$), and this was taken as evidence that Rh^{3+} and Rh^{4+} order over the two sites. The chemical composition requires Rh^{3+} and Rh^{4+} to coexist in a 4:1 ratio, which is the same as the ratio of the multiplicities of the two octahedral sites. The crystal structure is thus compatible with complete ordering of Rh^{3+} and Rh^{4+} in this mixed-valence compound.

We have now begun a program to synthesize new materials that are isostructural with $Ln_{18}Li_8Rh_5O_{39}$. Motivated by the observation of strong magnetic interactions in some K_4CdCl_6 compositions, our aim is to monitor the behavior of the cubic system when a significant concentration of paramagnetic cations is introduced into the network of six-coordinate polyhedra. Although the diamagnetic nature of Rh^{3+} ensures that no such behavior occurs in $Ln_{18}Li_8Rh_5O_{39}$, if aliovalent magnetic cations can be induced to occupy the different octahedral sites in an ordered manner, then the antiferromagnetic coupling between them might lead to the observation of ferrimagnetic behavior analogous to that observed in spinels. We describe below the attempted synthesis of $Ln_{18}Li_8M_5O_{39}$ (Ln = La, Pr, Nd, Sm; M = Mn, Fe, Co). As we shall show, this strategy has to date only been successful in the case of $Nd_{18}Li_8Fe_5O_{39}$, although we were also able to prepare $Nd_{18}Li_8Co_4O_{39}$. These two compositions have been studied in some detail by a combination of neutron diffraction, magnetometry, and Mössbauer spectroscopy.

Experimental Section

Attempts were made to synthesize pure samples of $Ln_{18}Li_8M_5O_{39}$ (Ln = La, Pr, Nd, Sm; M = Mn, Fe, Co). Stoichiometric quantities of oxide starting materials [lanthanum(III) oxide (99.999%, Alfa Aesar), praseodynium(III,IV) oxide (99.996%, Alfa Aesar), neodymium(III) oxide (99.99%, Alfa Aesar), samarium(III) oxide (99.998%, Alfa Aesar), manganese(IV) oxide (99.999%, Alfa Aesar), iron(III) oxide (99.998%, Alfa Aesar), cobalt(II,III) oxide (99.9985%, Alfa Aesar)] were ground together along with a 50% excess of the highly volatile lithium carbonate (AnalaR) prior to firing in pellet form at 800 °C in air overnight. A further 50% excess lithium carbonate was ground into the reaction mixture before it was fired again in air for 1 h, as a pellet, at 950 °C for $Nd_{18}Li_8Fe_5O_{39}$ and at 1000 °C for all other compositions. Powder X-ray diffraction was used to monitor the progress of the reactions. Further 1-h firings, with the addition of 50% excess lithium carbonate, were carried out on samples that powder X-ray diffraction showed to be impure at this stage.

All powder X-ray diffraction was carried out on a Philips X'pert diffractometer operating with Cu $K\alpha_1$ radiation with a step size of $\Delta 2\theta = 0.0084°$. High-intensity powder X-ray diffraction data were collected over a small angular range ($15° \le 2\theta \le 40°$) in order to detect lithium-containing impurities. High-resolution powder X-ray diffraction data for use in quantitative analysis were collected over the angular range $5° \le 2\theta \le 125°$. Limited Rietveld[12] refinement of the structures was carried out using the *GSAS*[13] suite of programs.

(10) Choi, Y. J.; Yi, H. T.; Lee, S.; Huang, Q.; Kiryukhin, V.; Cheong, S. W. *Phys. Rev. Lett.* **2008**, *100*, 047601.

(11) Frampton, P. P. C.; Battle, P. D.; Ritter, C. *Inorg. Chem.* **2005**, *44*, 7138.

(12) Rietveld, H. M. *J. Appl. Crystallogr.* **1969**, *2*, 65.

(13) Larson, A. C.; von Dreele, R. B. *General Structure Analysis System (GSAS)*; Los Alamos National Laboratories: Los Alamos, NM, 1994; LAUR 86-748.

Backgrounds were fitted using a Chebyshev polynomial of the first kind, and the peak shape was modeled using a pseudo-Voigt function.

Neutron powder diffraction data were collected on samples of $Nd_{18}Li_8Fe_5O_{39}$ and $Nd_{18}Li_8Co_4O_{39}$ using the diffractometer D2b at the Institut Laue Langevin, Grenoble, France. D2b is a high-flux, high-resolution instrument that operates at a wavelength of $\lambda = 1.591\ 47$ Å. Data were collected over the angular range $5° \leq 2\theta \leq 160°$ with a step size $\Delta 2\theta = 0.05°$ at room temperature and, for $Nd_{18}Li_8Fe_5O_{39}$ only, at 3.3 K. Samples (~0.5 g) were contained within vanadium cans ($\Phi = 5$ mm) and, for the low-temperature experiment, mounted in a Displex refrigerator. Rietveld refinements of the structures were carried out using the *FULLPROF*[14] program. Backgrounds were estimated manually and then refined using the software. Peak shapes were modeled using a pseudo-Voigt function employing three peak-asymmetry parameters in the angular region $2\theta \leq 54°$.

Magnetic measurements were carried out using a Quantum Design MPMS 5000 SQUID magnetometer. The magnetization (M) was measured as a function of the temperature upon warming from 2 to 300 K after cooling both in zero field (ZFC) and in the measuring field of 100 Oe (FC). The isothermal magnetization was measured as a function of the field (-50 kOe $\leq H \leq 50$ kOe) after cooling to the measuring temperature in 50 kOe. Alternating current (ac) susceptibility data were recorded at 11 frequencies (0.5 Hz $\leq \omega \leq$ 1000 Hz) in a direct field of ~2 Oe and an oscillating field of amplitude 3.5 Oe over the temperature range 3 K $\leq T \leq$ 9 K for $Nd_{18}Li_8Fe_5O_{39}$ and 2 K $\leq T \leq$ 6 K for $Nd_{18}Li_8Co_4O_{39}$ with $\Delta T =$ 0.1 K in each case.

The Mössbauer spectra have been measured between 4.2 and 295 K in a Janis Supervaritemp cryostat with a constant-acceleration spectrometer, which utilized a rhodium matrix cobalt-57 source and was calibrated at room temperature with α-iron powder. The Mössbauer spectral absorber contained 20 mg cm^{-2} of $Nd_{18}Li_8Fe_5O_{39}$ powder mixed with boron nitride. The ideal thickness of the Mössbauer absorber is limited to this value because of the strong nonresonant scattering of the γ-rays by the 18 neodymium ions per formula unit. This effect is, at least in part, responsible for the rather low signal-to-noise ratio observed between 4.2 and 12 K.

Results

To date, phase-pure samples of the composition $Ln_{18}Li_8Fe_5O_{39}$ have only been obtained for $Nd_{18}Li_8Fe_5O_{39}$. Attempted syntheses of $Ln_{18}Li_8M_5O_{39}$ (M = Mn, Co) were also unsuccessful. In these cases, Li_2MnO_3 or $LiCoO_2$ was observed to be present in the same molar percentage as the target compound, suggesting the formation of $Ln_{18}Li_8M_4O_{39}$ (M = Mn, Co). The synthesis described above was therefore repeated using a reactant stoichiometry appropriate for the formation of the metal-deficient composition. A phase-pure sample of $Nd_{18}Li_8Co_4O_{39}$ was obtained, but other cobalt- and manganese-containing compositions were contaminated by $LiCoO_2$ and Li_2MnO_3, respectively.

High-intensity X-ray diffraction data collected from the $Nd_{18}Li_8Fe_5O_{39}$ and $Nd_{18}Li_8Co_4O_{39}$ samples did not reveal any impurity phases. The patterns could be indexed in space group $Pm\bar{3}n$ with unit cell parameters $a = 11.97159(9)$ and 11.8564(2) Å for the iron- and cobalt-containing samples, respectively, consistent with the adoption of a $Ln_{18}Li_8Rh_5O_{39}$-like structure. However, in view of the dominance of the scattering by the heavier elements, a full structural analysis based on X-ray data was not attempted.

A more detailed structural analysis was carried out using the neutron diffraction data collected at room temperature. These revealed that lithium carbonate and lithium oxide were present as impurity phases at a level of less than 1 wt % in $Nd_{18}Li_8Fe_5O_{39}$. Initial refinements in the space group $Pm\bar{3}n$ using a structural model based on $La_{18}Li_8Rh_5O_{39}$ gave reasonable fits to the data, but the displacement parameters for the midchain octahedral sites at ($^1/_4$, $^1/_4$, $^1/_4$), the trigonal-prismatic sites at (x, x, x) where $x \sim 0.375$, and the disordered oxide ions (O4) forming the octahedra around the chain-intersection sites refined to large values. To account for this, the octahedra at ($^1/_4$, $^1/_4$, $^1/_4$) and the trigonal prisms were allowed to contain both lithium and iron cations. Models with different occupational constraints on the system were considered, but it was found that the best fit was achieved when both the octahedral and trigonal-prismatic sites were fully occupied and hence the stoichiometry $Nd_{18}Li_8Fe_5O_{39}$ was maintained. Different models for the O4 sites were considered. First, oxygen vacancies were introduced with the site constrained to occupy the ideal (x, 0, 0) position, and second the fully occupied site was allowed to disorder onto a general position (x, y, z). It was found that the most satisfactory model had ~10% of the iron occupying trigonal-prismatic sites and a disordered O4 position. However, the final displacement parameter of O4, although reduced, is still large. No problems were encountered in refining the parameters associated with the atoms (Nd1, Nd2, O2, and O3), which form the framework within which the chains are contained. The refined structural parameters and the most significant bond lengths and bond angles are listed in Tables 1 and 2, respectively; the observed and calculated neutron diffraction patterns are shown in Figure 3. Neutron diffraction data collected at 3.3 K show no significant changes in intensity or additional peaks compared to those collected at room temperature (Figure 3). Refinement of the low-temperature structure was carried out with the same constraints and structural model as were used in the analysis of the room temperature data and gave, within error, the same cation distribution on the chain sites (Table 1). Even at 3.3 K, the displacement parameter of the O4 site is observed to be large. This is consistent with the presence of incompletely modeled static disorder around this site.

The neutron diffraction data collected from $Nd_{18}Li_8Co_4O_{39}$ at room temperature were also analyzed using the space group $Pm\bar{3}n$. The structure of $Ln_{18}Li_8Rh_5O_{39}$ was again taken as a starting model but with cation vacancies on both of the octahedral sites to ensure the correct stoichiometry. Preliminary refinement of the occupation factors of the two octahedral sites showed a strong preference for that at the origin to be fully occupied by cobalt. In subsequent refinements, this site was therefore constrained to be fully occupied, with the remaining cobalt occupying 75% of the midchain octahedral sites at ($^1/_4$, $^1/_4$, $^1/_4$). Structural models in which

(14) Rodriguez-Carvajal, J. *Physica B* **1993**, *192*, 55.

Table 1. Structural Parameters of $Nd_{18}Li_8Fe_5O_{39}$ in Space Group $Pm\bar{3}n$ at Room Temperature and 3.3 K

		room temperature	3.3 K
a/Å		11.96687(1)	11.93868(1)
R_p, χ^2		0.041, 2.5	0.048, 2.6
Nd1 24*k* (0, *y*, *z*)	*y*	0.3076(3)	0.3073(3)
	z	0.3054(3)	0.3059(3)
	B_{iso}/Å^2	0.32(4)	0.47(4)
Nd2 12*f* (*x*, 0, 0)	*x*	0.3486(3)	0.3490(3)
	B_{iso}/Å^2	0.00(5)	0.20(6)
Fe1 2*a* (0, 0, 0)	B_{iso}/Å^2	0.19(11)	0.13(12)
Fe2(Li) 8*e* ($^1/_4$, $^1/_4$, $^1/_4$)	B_{iso}/Å^2	1.13(9)	1.47(10)
	Li occupancy	0.15(1)	0.15(1)
	Fe occupancy	0.85(1)	0.85(1)
Li1(Fe) 16*i* (*x*, *x*, *x*)	*x*	0.3683(9)	0.3681(10)
	B_{iso}/Å^2	0.1(4)	0.4(4)
	Li occupancy	0.926(5)	0.926(5)
	Fe occupancy	0.074(5)	0.074(5)
O1 48*l* (*x*, *y*, *z*)	*x*	0.8651(3)	0.8653(3)
	y	0.8606(3)	0.8603(3)
	z	0.6931(2)	0.6930(2)
	B_{iso}/Å^2	0.68(4)	0.85(4)
O2 6*d* ($^1/_4$, $^1/_2$, 0)	B_{iso}/Å^2	0.59(12)	0.20(11)
O3 12*g*	*x*	0.6322(5)	0.6313(5)
(*x*, 0, $^1/_2$)	B_{iso}/Å^2	0.50(9)	0.55(9)
O4 48*l* (*x*, *y*, *z*)	*x*	0.1531(7)	0.1525(8)
	y	0.015(2)	0.0209(16)
	z	0.019(2)	0.011(3)
		2.6(3)	2.9(4)
	B_{iso}/Å^2 occupancy	$^1/_4$	$^1/_4$

Table 2. Bond Lengths (Å) and Bond Angles (deg) in $Nd_{18}Li_8Fe_5O_{39}$ at Room Temperature and 3.3 K

	room temperature	3.3 K
Nd1−O1	2.500(4) × 2	2.492(4) × 2
	2.580(5) × 2	2.567(5) × 2
	2.636(4) × 2	2.638(4) × 2
Nd1−O2	2.429(4)	2.416(4)
Nd1−O3	2.420(4)	2.420(4)
	3.098(4)	3.104(4)
Nd2−O1	2.374(3) × 4	2.370(3) × 4
Nd2−O3	2.405(5) × 2	2.389(5) × 2
Nd2−O4	2.358(11)	2.363(11)
Fe1−O4	1.855(9) × 6	1.842(9) × 6
Fe2(Li)−O1	2.028(3) × 6	2.023(3) × 6
Li1(Fe)−O1	2.099(11) × 3	2.093(12) × 3
Li1(Fe)−O4	2.25(2)[a]x3	2.25(2)[a]x3
Li1(Fe)−Li1(Fe)	3.152(15)	3.149(17)
Fe1−Li1(Fe)	2.730(11)	2.727(12)
Fe2(Li)−Li1(Fe)	2.452(11)	2.442(12)
O1−Fe2(Li)−O1	90.2(2)	90.3(2)
	88.3(2)	88.8(2)
	91.4(2)	91.4(2)

[a] The average bond length to a disordered oxygen position.

lithium was allowed to occupy the vacant cation sites were considered. These analyses provided no evidence for the presence of lithium in the octahedral sites, even when the composition of the phase was allowed to vary to incorporate additional lithium. The presence of vacancies on all four oxygen sites was also considered, but no evidence for an oxygen deficiency was observed and the composition was finally constrained to be $Nd_{18}Li_8Co_4O_{39}$. Profile analysis then resulted in good agreement between the observed and calculated diffraction patterns (Figure 4). As in the case of $Nd_{18}Li_8Fe_5O_{39}$, the O4 site, which links the trigonal prisms and the central octahedron, was found to be disordered, although, in contrast to the Fe-containing compound, the disorder was modeled with a displacement

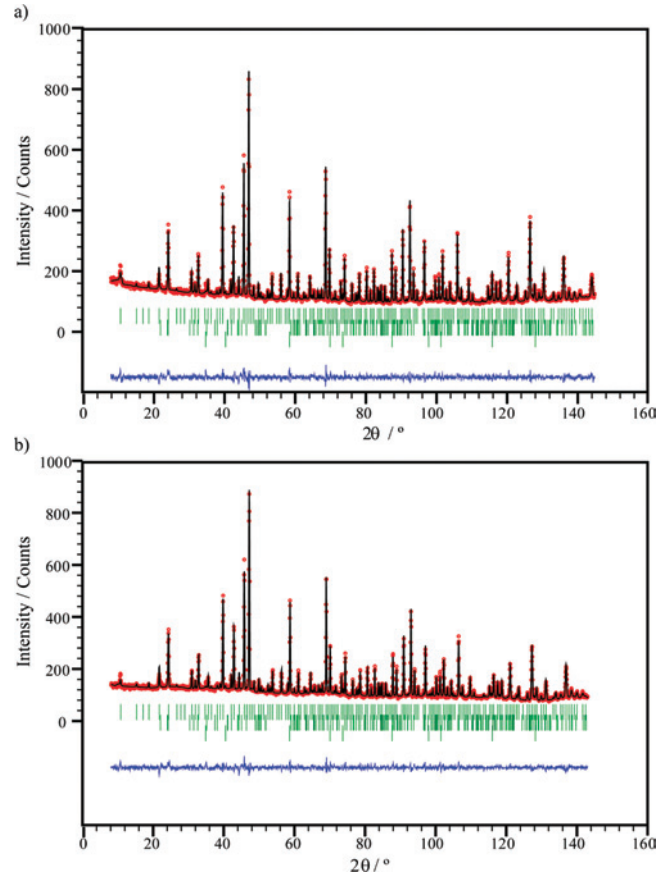

Figure 3. Observed (○) and calculated (—) neutron diffraction profiles for $Nd_{18}Li_8Fe_5O_{39}$ at (a) room temperature and (b) 3.3 K. Difference curves are also shown. Reflection positions for the main phase (upper), lithium carbonate (middle), and lithium oxide (lower) are indicated by vertical lines.

to (*x*, 0, *z*) rather than to (*x*, *y*, *z*); there was no significant improvement in the fit when the additional variable was introduced. The atomic displacement parameter associated with the disordered O4 site was again large (Table 3). The most significant bond lengths and bond angles in $Nd_{18}Li_8Co_4O_{39}$ are listed in Table 4.

The temperature dependence of the direct current (dc) molar magnetic susceptibility of $Nd_{18}Li_8Fe_5O_{39}$ (Figure 5) reveals a magnetic transition at $T_f = 5.75$ K, where the ZFC and FC susceptibilities reach a maximum. Below the transition, both the ZFC and FC susceptibilities are observed to decrease until $T \sim 4$ K, at which temperature the FC susceptibility becomes independent of the temperature. Above T_f, the inverse susceptibility is linear, and fitting to the Curie−Weiss law for $T > 100$ K gives $C = 43.67(4)$ emu mol^{-1} and $\theta = -28.0(2)$ K. At 2 K, the field dependence of the isothermal magnetization shows (Figure 6) narrow hysteresis behavior below $H = 5$ kOe. No saturation of the magnetization is observed, even in the maximum measuring field of 50 kOe.

The ZFC and FC dc susceptibilities of $Nd_{18}Li_8Co_4O_{39}$ diverge slightly below 10 K (Figure 7) and a magnetic transition is signaled by a maximum in both at $T_N = 2.3$ K. At high temperatures, the inverse susceptibility is a linear function of the temperature, and fitting to the Curie−Weiss law at $T > 100$ K gives $C = 32.13(5)$ emu mol^{-1} and $\theta =$

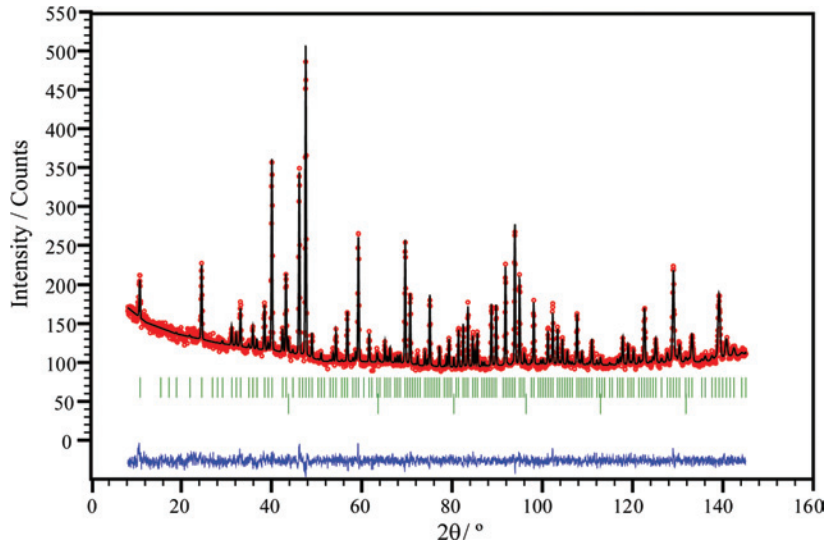

Figure 4. Observed (○) and calculated (—) neutron diffraction profiles for $Nd_{18}Li_8Co_4O_{39}$ at room temperature. Difference curves are also shown. Reflection positions for the main phase (upper) and vanadium (lower) are indicated by vertical lines.

Table 3. Structural Parameters of $Nd_{18}Li_8Co_4O_{39}$ in Space Group $Pm\bar{3}n$ at Room Temperature

a/Å		11.85014(2)
R_p, χ^2		0.066, 1.6
Nd1 24*k* (0, y, z)	*y*	0.3061(4)
	z	0.3027(4)
	B_{iso}/Å^2	0.38(5)
Nd2 12*f* (*x*, 0, 0)	*x*	0.3480(4)
	B_{iso}/Å^2	0.21(6)
Co1 2*a* (0, 0, 0)	B_{iso}/Å^2	−0.2(5)
Co2 8*e* ($^1/_4$, $^1/_4$, $^1/_4$)	B_{iso}/Å^2	0.7(3)
	occupancy	$^3/_4$
Li1 16*i* (*x*, *x*, *x*)	*x*	0.3696(8)
	B_{iso}/Å^2	1.3(3)
O1 48*l* (*x*, *y*, *z*)	*x*	0.8626(4)
	y	0.8585(4)
	z	0.6958(3)
	B_{iso}/Å^2	0.75(5)
O2 6*d* ($^1/_4$, $^1/_2$, 0)	B_{iso}/Å^2	1.2(2)
O3 12*g* (*x*, 0, $^1/_2$)	*x*	0.6310(6)
	B_{iso}/Å^2	0.68(11)
O4 24*k* (*x*, 0, *z*)	*x*	0.1524(8)
	z	−0.017(2)
	B_{iso}/Å^2	2.8(3)
	occupancy	$^1/_2$

Table 4. Bond Lengths (Å) and Bond Angles (deg) in $Nd_{18}Li_8Co_4O_{39}$ at Room Temperature

Nd1−O1	2.541(6) × 2
	2.579(5) × 2
	2.505(5) × 2
Nd1−O2	2.431(5)
Nd1−O3	2.431(5)
	3.069(5)
Nd2−O1	2.394(4) × 4
Nd2−O3	2.378(6) × 2
Nd2−O4	2.327(11)
Co1−O4	1.817(11) × 6
Co2−O1	1.961(4) × 6
Li1−O1	2.065(11) × 3
Li1−O4	2.21(2)[a] × 3
Li1−Li1	3.091(13)
Co1−Li1	2.676(9)
Co2−Li1	2.455(9)
O1−Co2−O1	89.5(3)
	89.1(3)
	91.9(3)

[a] The average bond length to a disordered oxygen position.

−46.6(3) K. The results of isothermal magnetization measurements carried out at three temperatures are shown in Figure 8. Data were collected at 12 K, which is above the temperature at which the ZFC and FC susceptibilities diverge, at 4 K, which is below the divergence temperature, and at 2 K, which is below T_N. The irreversibility revealed in Figure 7 is too small to be apparent on the scale of Figure 8. However, at temperatures below 12 K, the susceptibility (*M*/*H*) decreases in the highest fields.

The temperature dependence of the ac susceptibility of $Nd_{18}Li_8Fe_5O_{39}$ shows (Figure 9) a significant shift in the maximum of the real susceptibility, χ', with frequency; T_f(0.5 Hz) = 5.1 K; T_f(1000 Hz) = 5.8 K. The shift in the transition temperature can be parametrized as the ratio of the relative change in the freezing temperature to the decadic shift in frequency, $\Delta T_f/T_f \Delta \log \omega$,[15] which takes a value of 0.037. A maximum in the imaginary susceptibility, χ'', is also observed close to the transition temperature, and for all frequencies, the minimum in $d\chi''/dT$ is observed to be coincident with the maximum value of χ'.

The real part of the ac susceptibility of $Nd_{18}Li_8Co_4O_{39}$ shows (Figure 10) shows no frequency dependence across the measured temperature range and T_N = 2.3 K for all measuring frequencies. The imaginary component of the susceptibility, χ'', does not deviate significantly from zero across the measured temperature range.

The iron-57 Mössbauer spectra of $Nd_{18}Li_8Fe_5O_{39}$ obtained between 12 and 295 K (Figure 11) reveal that $Nd_{18}Li_8Fe_5O_{39}$ is paramagnetic above 25 K and exhibits more complex magnetic behavior at and below ca. 12 K. The paramagnetic spectra obtained at and above 25 K have been fit with three doublets assigned to the 2*a*, 8*e*, and 16*i* sites, with relative areas constrained to 19.99, 68.17, and 11.84%, respectively, the iron occupancies of these sites as determined by neutron diffraction and given in Table 1. The resulting fits (see Figure 11) and the corresponding spectral parameters, given in Table 5, may not be unique, but they are most consistent with the

(15) Mydosh, J. A. *Spin glasses: an experimental introduction*; Taylor & Francis: London, 1993.

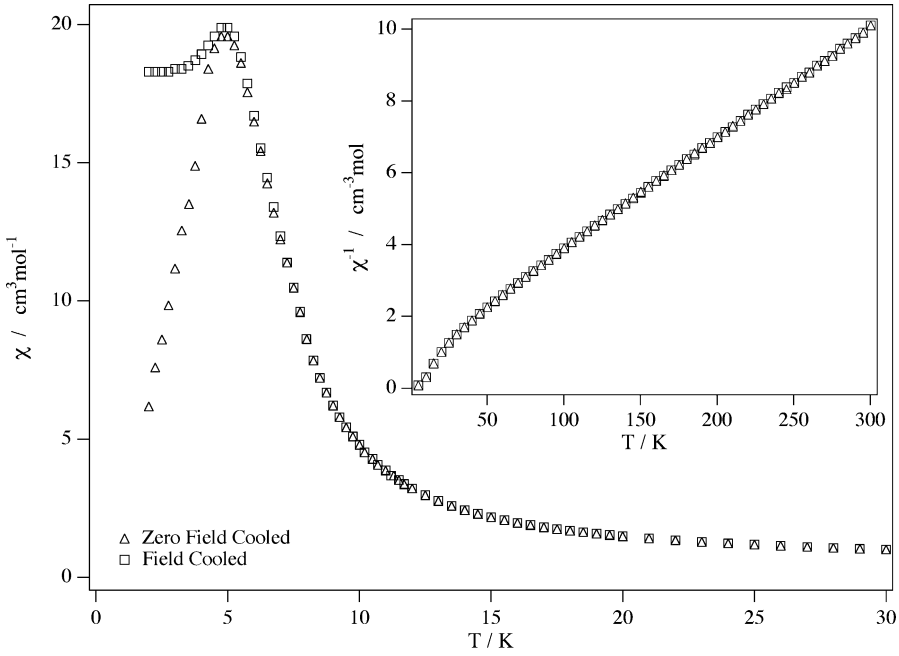

Figure 5. Temperature dependence of the molar dc magnetic susceptibility of $Nd_{18}Fe_5Li_8O_{39}$ measured in 100 Oe. The inverse susceptibility is inset.

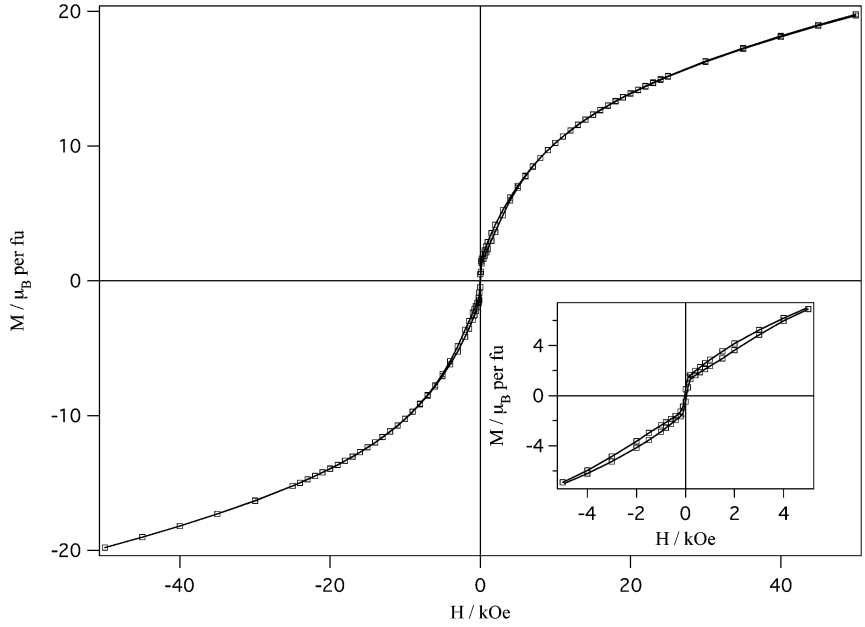

Figure 6. Field dependence of the magnetization per formula unit of $Nd_{18}Fe_5Li_8O_{39}$ at 2 K.

electronic properties of $Nd_{18}Li_8Fe_5O_{39}$, which, at least formally, should contain four Fe^{III} ions and one Fe^{IV} ion per formula unit.

Between 12 and 8 K, the fits involve a complex superposition of paramagnetic, slowly relaxing and static components; their isomer shifts have been constrained to be consistent with those observed at 25 and 4.2 K. The 12 K spectrum of $Nd_{18}Li_8Fe_5O_{39}$ has been measured over velocity ranges of ± 3 and ± 12 mm s^{-1}, and the fits of these spectra, shown at the bottom of Figure 11 and the top of Figure 12 were achieved using the same model. In addition to the paramagnetic components observed at 25 K, the 12 K spectra clearly indicate the presence of both static spins and spins that show slow magnetic relaxation on the time scale of the Mössbauer experiment. The paramagnetic components have been fit with the same relative areas and hyperfine parameters as those observed at 25 K. The static spins give rise to the red sextet observed between -8 and $+9$ mm s^{-1} with a field of 51.0 T and a relative area of ca. 40%; this is assigned to the 8*e* site. It is also apparent from the 12 K spectrum at the bottom of Figure 11 that the spectrum is broadened between -1 and $+2$ mm s^{-1} as a result, most likely, of a transferred hyperfine field experienced by some of the iron on the 2*a* and 8*e* sites. The relative areas of the two additional components needed to model this effect are 3.5 and 20.5% of the total spectral area at 12 K; the corresponding transferred fields are 0.8 and 3.8 T, respectively. The iron atoms on the 16*i* site appear to be paramagnetic at this temperature.

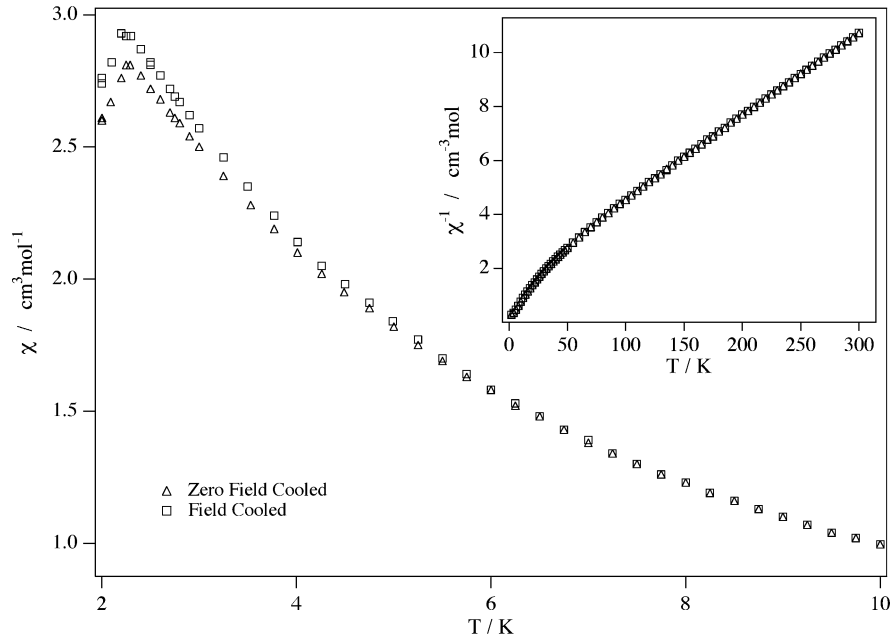

Figure 7. Temperature dependence of the molar dc magnetic susceptibility of $Nd_{18}Co_4Li_8O_{39}$ measured in 100 Oe. The inverse susceptibility is inset.

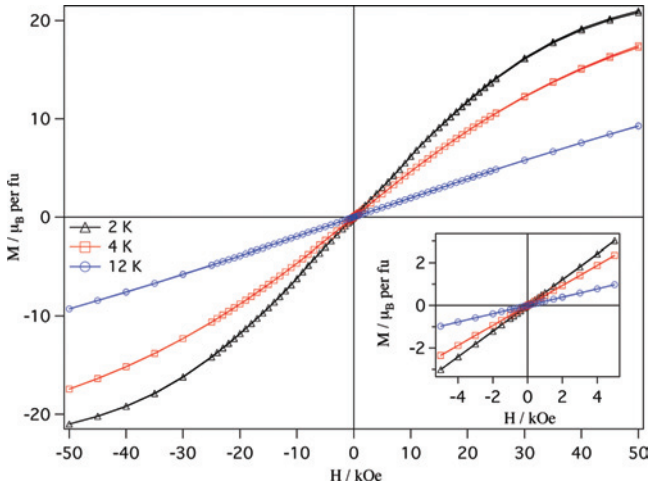

Figure 8. Field dependence of the magnetization per formula unit of $Nd_{18}Co_4Li_8O_{39}$ at selected temperatures.

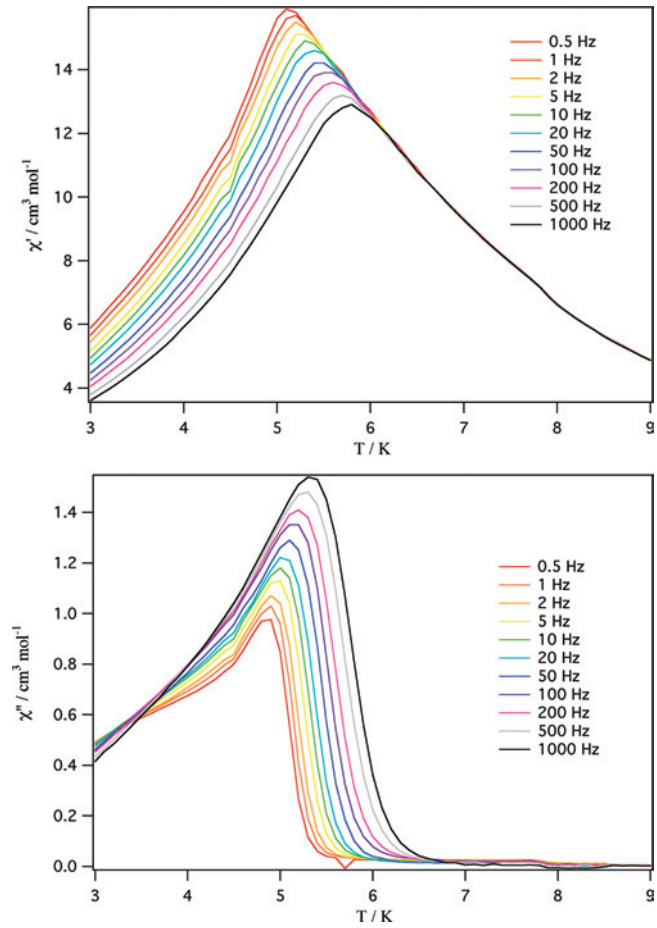

Figure 9. Real (upper) and imaginary (lower) molar ac susceptibility of $Nd_{18}Fe_5Li_8O_{39}$ as a function of the temperature and frequency.

At 10 K, some spins on the 8*e* and 16*i* sites show either static or slow relaxation on the Mössbauer time scale; they contribute sextets with fully developed hyperfine fields with a total relative area of ca. 40%. Two broad components with small hyperfine fields of 1.8 and 6.0 T are assigned to the 2*a* and 8*e* sites experiencing intermediate relaxation on the Mössbauer time scale; their relative area is ca. 52%. One unresolved paramagnetic doublet with hyperfine parameters characteristic of the 8*e* site has a relative area of 8%. Hence, with decreasing temperature from 12 to 10 K, the relative fraction of iron ions experiencing intermediate relaxation increases, at the expense of the fraction of paramagnetic ions. At 8 K, the spins on 59% of the iron ions are static, or exhibit only slow relaxation, and contribute sextets with fully developed hyperfine fields, whereas 41% of the iron ions exhibit intermediate relaxation and contribute to the broad absorption observed at 8 K; see Figure 12. The resolution of the Mössbauer spectrum does not allow the determination of the eventual remaining paramagnetic contribution, if any. Hence, between 10 and 8 K, the relaxation is slowing and a larger relative fraction of iron ions is experiencing static or slow relaxation.

The 4.2 K spectrum has been fit with the superposition of three sextets, with hyperfine fields of 20.3(3), 51.6(1), and

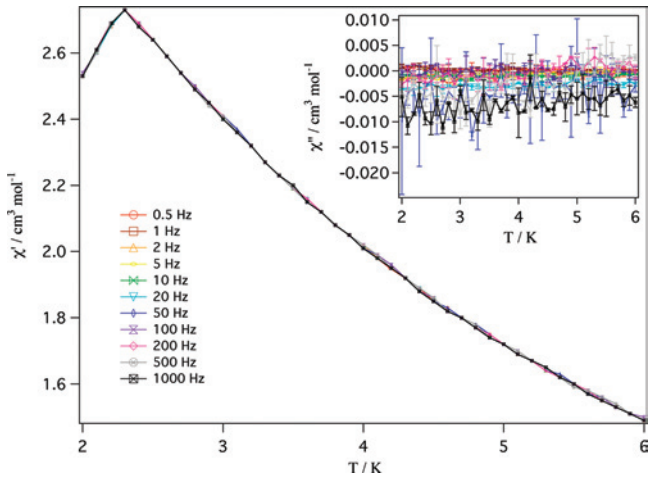

Figure 10. Real and imaginary (inset) molar ac susceptibility of $Nd_{18}Co_4Li_8O_{39}$ as a function of the temperature and frequency.

47.3(7) T, assigned to the 2*a*, 8*e*, and 16*i* sites, respectively, with the relative areas constrained to the iron occupancy of these sites determined by neutron diffraction and given above. The remaining spectral parameters of these sextets are given in Table 5. Both isomer shifts and hyperfine fields[16] are compatible with the presence of low-spin Fe^{IV} on the 2*a* site and high-spin Fe^{III} on the 8*e* and 16*i* sites.

Support for the Mössbauer spectral fits described above may be obtained through the temperature dependence of the isomer shifts and quadrupole splittings observed for the 2*a*, 8*e*, and 16*i* sites and their weighted average values, shown in Figures 13 and 14, respectively. As expected, the three isomer shifts decrease with increasing temperature because of the second-order Doppler shift.[17] A fit with the Debye model yields the solid line fits shown in Figure 13 and Debye temperatures of 830(40), 580(20), 650(30), and 620(20) K for the 2*a*, 8*e*, and 16*i* site isomer shifts and their weighted average, respectively. The higher value for the 2*a* site results because this is the iron(IV) site with shorter bonds and the corresponding higher vibrational frequencies.

Between 25 and 295 K, the quadrupole splittings of the 8*e* and 16*i* sites are virtually constant, whereas the quadrupole splitting of the 2*a* site decreases slightly with increasing temperature. As a consequence, in the fitting of the 4.2 K spectrum (see Figure 12), the values of the quadrupole splitting have been constrained to the values given in Table 5 and the values of θ, the angle between the principal axis of the electric field gradient and the magnetic hyperfine field,

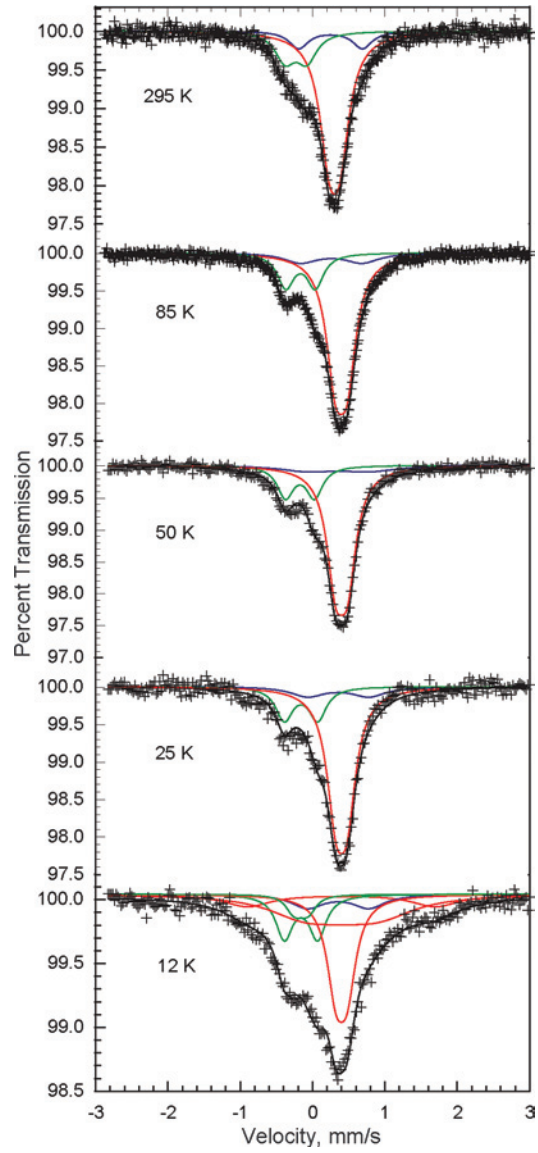

Figure 11. Iron-57 Mössbauer spectra of $Nd_{18}Fe_5Li_8O_{39}$ obtained at the indicated temperatures. The green, red, and blue lines indicate the components assigned to the 2*a*, 8*e*, and 16*i* sites, respectively. This color scheme matches that used in Figure 2.

have been adjusted. The resulting values are 22, 42, and 56° for the 2*a*, 8*e*, and 16*i* sites, respectively. These θ values lead to virtually zero quadrupole shifts and nearly symmetric sextets for the 8*e* and 16*i* sites and to a positive quadrupole shift for the 2*a* site, a shift that is clearly visible in Figure

Table 5. Mössbauer Spectral Parameters for $Nd_{18}Li_8Fe_5O_{39}$

		2*a* site			8*e* site			16*i* site	
T/K	δ^a/mm s^{-1}	ΔE_Q/mm s^{-1}	Γ/mm s^{-1}	δ^a/mm s^{-1}	ΔE_Q/mm s^{-1}	Γ/mm s^{-1}	δ^a/mm s^{-1}	ΔE_Q/mm s^{-1}	Γ/mm s^{-1}
295	−0.229(9)	0.30(2)	0.33(2)	0.306(1)	0.149(8)	0.332(7)	0.27(1)	0.88(3)	0.33(3)
225	−0.195(5)	0.38(1)	0.33(1)	0.345(1)	0.167(4)	0.337(6)	0.309(7)	0.84(2)	0.33(2)
155	−0.162(4)	0.409(7)	0.286(8)	0.380(1)	0.179(3)	0.327(5)	0.341(8)	0.91(2)	0.36(2)
100	−0.155(6)	0.44(2)	0.28(1)	0.39(1)	0.18(2)	0.31(1)	0.36	0.88	0.46
85	−0.167(4)	0.408(8)	0.278(8)	0.395(1)	0.164(3)	0.307(6)	0.35(2)	0.85(3)	0.56(5)
85	−0.161(3)	0.422(8)	0.262(7)	0.397(1)	0.167(3)	0.286(4)	0.35	0.85	0.38(2)
75	−0.169(4)	0.42(5)	0.28(1)	0.395(2)	0.164(3)	0.30(1)	0.35	0.85	0.80(3)
50	−0.163(4)	0.44(4)	0.27(2)	0.404(2)	0.164(2)	0.30(1)	0.35	0.85	0.93(5)
25	−0.160(3)	0.46(4)	0.29(2)	0.399(3)	0.154(3)	0.32(2)	0.35	0.85	0.57(2)
4.2	−0.159(4)	0.47	0.45(8)	0.404(2)	0.18	0.51(5)	0.366(5)	0.85	0.52(16)

[a] The isomer shifts are given relative to room temperature α-iron powder. If no error is indicated, the parameter has been constrained to the value given.

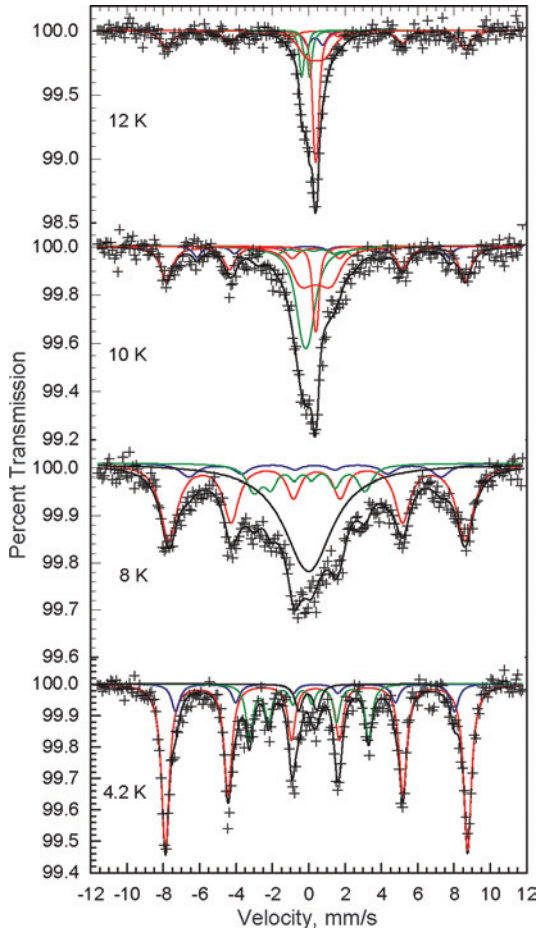

Figure 12. Iron-57 Mössbauer spectra of $Nd_{18}Fe_5Li_8O_{39}$ obtained at the indicated temperatures. The green, red, and blue lines indicate the components assigned to the 2*a*, 8*e*, and 16*i* sites, respectively. The black line in the 8 K spectrum represents the combined contribution from spins showing an intermediate relaxation rate.

12. The 4.2 K line widths are between 0.45 and 0.52 mm s^{-1}, and thus there is a significant broadening as compared to both the line widths observed above 25 K and the typical experimental line width of 0.28 mm s^{-1} of the external lines of the calibration spectra.

Discussion

The results presented above demonstrate that elements from the first-row of the d block can be introduced into the structure previously observed for $La_{18}Li_8Rh_5O_{39}$. However, it appears either that the introduction of smaller transition-metal cations requires the use of smaller lanthanide elements to create the framework within which the polyhedral chains reside or that the synthesis conditions must be tailored precisely to the particular combination of elements used and that we have not yet found the correct conditions for the synthesis of compositions containing the larger lanthanides, for example, $La_{18}Li_8Fe_5O_{39}$. Our results also show that the structure is able to accommodate vacancies on the transition-metal sublattice, as exemplified by $Nd_{18}Li_8Co_4O_{39}$.

The fits shown in Figure 3 indicate that we have produced a good overall description of the structure of $Nd_{18}Li_8Fe_5O_{39}$ at both room temperature and 3.3 K. However, the high values refined for the atomic displacement parameters of

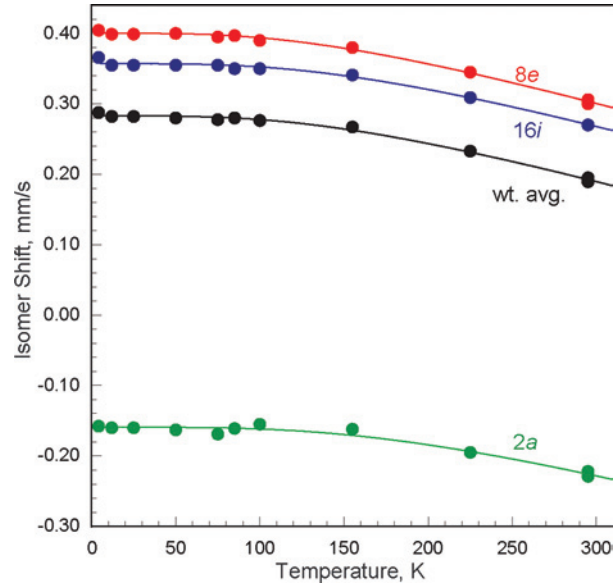

Figure 13. Temperature dependence of the Mössbauer isomer shifts for the 2*a*, 8*e*, and 16*i* sites and their weighted average in $Nd_{18}Fe_5Li_8O_{39}$. The solid lines correspond to a fit with the Debye model for a solid. The error bars are at most the size of the data points.

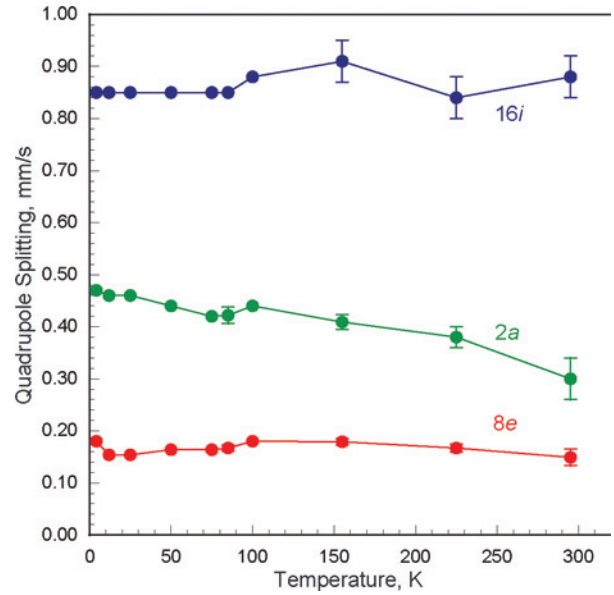

Figure 14. Temperature dependence of the Mössbauer quadrupole splittings for the 2*a*, 8*e*, and 16*i* sites in $Nd_{18}Fe_5Li_8O_{39}$. The absence of error bars indicates either that the quadrupole splitting was fixed (see Table 5) or that the error is less that the size of the data points.

Fe2(Li) and O4 indicate the presence of residual disorder that we have not been able to model in detail using our neutron diffraction data. The coordination geometry around the Nd1 and Nd2 sites in $Nd_{18}Li_8Fe_5O_{39}$ is similar to that observed previously around the corresponding sites in $La_{18}Li_8Rh_5O_{39}$; the bond lengths are consistent with those found in the perovskite $NdFeO_3$.[18] We assign the iron cations occupying the 8*e* and 16*i* sites as high-spin Fe^{3+}. This is consistent with the relatively large and positive isomer shifts derived from the Mössbauer spectra.[16,19] The quadrupole splitting of the 8*e* site is typical of Fe^{3+}, whereas that of the 16*i* site is rather large for this cation. The Fe2(Li)−O1 distance (2.028 Å) is slightly longer than what might be

expected for an $Fe^{3+}-O$ distance in a mixed-metal oxide, consistent with the presence of some Li^+ cations on the 8*e* site. This site-exchange disorder requires the concomitant transfer of an equal quantity of Fe^{3+} to the lithium-dominated prismatic 16*i* site. The Li1(Fe)−O1 distance (2.099 Å) in the trigonal prism lies within the expected range for a Li−O bond and is much shorter than the mean Li1(Fe)−O4 distance. The displacement of the cation from the midpoint of the prism is consistent with the relatively large quadrupole splitting observed in the Mössbauer spectra. The Fe1−O4 distance around the 2*a* site (1.855 Å) is short enough to suggest that the cation is Fe^{4+} in a low-spin state. The Curie constant [43.67(4) emu mol^{-1}] derived from our dc susceptibility data is actually lower than the value (46.98) predicted to arise from the Nd^{3+} ($J = {}^9/_2$) and Fe^{3+} ($S = {}^5/_2$) cations alone, and it is therefore impossible to use these data to glean further evidence concerning the spin state of the Fe^{4+} cations. The reduction in the value of the Curie constant might be attributable to spin pairing between magnetic cations in face-sharing coordination polyhedra centered on the 16*i* and 8*e* sites. The short Fe−Fe contacts that cause this coupling arise as a consequence of the lithium/iron site exchange. Although the magnetic data are unhelpful, further evidence to support our spin-state assignment comes from a previous study by Mössbauer spectroscopy of the Fe^{4+}-containing perovskite $CaFeO_3$. Takano et al.[20] recorded spectra at pressures of up to 50 GPa and observed a transition from high-spin Fe^{4+} to low-spin Fe^{4+} at ∼30 GPa at room temperature. The mean pseudocubic unit-cell parameter decreased upon application of pressure, but in the high-spin phase at ambient pressure, it was slightly larger (3.76 Å) than the value of ∼3.71 Å that would correspond to an Fe−O bond length of 1.855 Å. The Mössbauer isomer shift decreased from ∼0.07 mm s^{-1} for the high-spin cation to ∼−0.2 mm s^{-1} for the low-spin form, and an internal hyperfine field of ∼16 T was measured for the latter state. Thus, the observed Fe1−O4 bond length, the hyperfine field, the high Debye temperature, and, in particular, the isomer shift at the 2*a* site are all consistent with our assignment of Fe1 as low-spin Fe^{4+}. Although the presence of lithium/iron disorder over the 16*i*/8*e* sites renders the structure of $Nd_{18}Li_8Fe_5O_{39}$ somewhat more complex than that of $La_{18}Li_8Rh_5O_{39}$, the neutron diffraction data and Mössbauer spectra together show that the tetravalent cation is again located entirely on the 2*a* site. In this sense, the cation ordering seen in the rhodium phase is maintained in $Nd_{18}Li_8Fe_5O_{39}$.

The chemistry of $Nd_{18}Li_8Co_4O_{39}$ must be interpreted without the insight provided by Mössbauer spectroscopy. The cation-deficient nature of this composition requires all of the cobalt cations to be in the 4+ oxidation state. Although it is relatively straightforward to prepare oxides, for example, the hexagonal chain compound $Sr_6Co_5O_{15}$,[21] in which the mean oxidation state of the cobalt cations is greater than 3+, it is difficult to prepare fully oxidized Co^{4+} compounds at ambient pressure.[22] However, our neutron diffraction study showed all of the oxide sites to be fully occupied, and we therefore have no direct evidence for the presence of reduced (Co^{3+}) cations. The electropositive cations in $Nd_{18}Li_8Co_4O_{39}$ will not compete strongly for the negative charge density of the anions, and we suggest that it is the high concentration of the former that allows stabilization of Co^{4+}. The mean bond lengths around the Nd1 and Nd2 sites in this compound are very similar to those found in the iron-containing analogue. The Co−O distance around the 2*a* site (1.817 Å) is shorter than that in the 2H perovskite $BaCoO_3$ (1.874 Å)[23] and is comparable to the Fe−O distance in the high-pressure form of $CaFeO_3$ referred to above. The structures of both compounds described in this account thus appear to exert a chemical pressure on the 2*a* site that is equivalent to a mechanical pressure of ∼30 GPa. The small atomic displacement parameter of Co1 on the 2*a* site is a consequence of the compactness of the coordination environment. In contrast to $Nd_{18}Li_8Fe_5O_{39}$, there is no site exchange between lithium and the transition metal in $Nd_{18}Li_8Co_4O_{39}$, possibly because the 8*e* site is too small (Co2−O1 = 1.961 Å) to accommodate Li^+. Although too small to accommodate Li^+, the 8*e* site is large enough to accommodate a high-spin transition-metal cation. However, in the absence of short (∼2.5 Å) Co−Co contacts resulting from site exchange, the high-temperature Curie constant is expected to be a reliable indicator of the cobalt spin state, and the observed value (32.13 emu mol^{-1}) compares well with that expected (30.98 emu mol^{-1}) if all of the Co^{4+} cations are in a low-spin state. We therefore conclude, despite the relatively long Co2−O1 distance, that the low-spin configuration is adopted.

The inequality of the ZFC and FC susceptibilities of $Nd_{18}Li_8Fe_5O_{39}$ at low temperatures suggests that this compound behaves like a spin glass below $T_f = 5.75$ K. The steady decrease in the ZFC susceptibility upon cooling below T_f suggests that the magnetic moments associated with all of the magnetic cations (Nd^{3+}, Fe^{3+}, and Fe^{4+}) are involved in the freezing process. The hysteresis observed in the field dependence of the magnetization (Figure 6) is consistent with spin-glass-like behavior, as is the absence of magnetic Bragg scattering in the neutron diffraction pattern collected at 3.3 K. The frequency dependence of T_f in the ac susceptibility (Figure 9) provides further evidence, and the value (0.037) deduced for the ratio of the relative change in the freezing temperature to the decadic shift in frequency is typical of an insulating spin glass. The broadened spectral lines in the 4.2 K Mössbauer spectrum of $Nd_{18}Li_8Fe_5O_{39}$ are also

(16) Russo, U.; Long G. J. In *Mossbauer Spectroscopy Applied to Inorganic Chemistry*; Long, G. J., Grandjean, F., Eds.; Plenum Press: New York, 1989; Vol. *3*, p 289.
(17) Shenoy G. K.; Wagner F. E.; Kalvius, G. M. In *Mossbauer Isomer Shifts*; Shenoy, G. K., Wagner, F. E., Eds.; North-Holland: Amsterdam, The Netherlands, 1978; p 49.
(18) Marezio, M.; Remeika, J. P.; Dernier, P. D. *Acta Crystallogr.* **1970**, *B26*, 2008.
(19) Ingalls, R.; VanderWoude, F.; Sawatzky, G. A. In *Mossbauer Isomer Shifts*; Shenoy, G. K., Wagner, F. E., Eds.; North-Holland: Amsterdam, The Netherlands, 1978; p 361.
(20) Takano, M.; Nasu, S.; Abe, T.; Yamamoto, K.; Endo, S.; Takeda, Y.; Goodenough, J. B. *Phys. Rev. Lett.* **1991**, *67*, 3267.
(21) Harrison, W. T. A.; Hegwood, S. L.; Jacobson, A. J. *J. Chem. Soc., Chem. Commun.* **1995**, 1953.
(22) Shimada, M.; Takeda, Y.; Taguchi, H.; Kanamaru, F.; Koizumi, M. *J. Cryst. Growth* **1975**, *29*, 75.
(23) Taguchi, H.; Takeda, Y.; Kanamaru, F.; Shimada, M.; Koizumi, M. *Acta Crystallogr., Sect. B* **1977**, *33*, 1299.

consistent with an array of frozen spins, as are the very small quadrupole shifts. The random orientation of the spins and of the hyperfine fields relative to the crystallographic axes will lead to a distribution of θ angles. This distribution is actually taken into account by the broadened line widths and an average value of the θ angle, a combination that leads to a virtually zero quadrupole shift. Finally, the evolution of the Mössbauer spectrum, particularly the outer lines, with temperature shows that we are observing spin freezing rather than the onset of long-range magnetic order. The outer lines are visible at 12 K (Figure 12), and their separation is then very close to that observed at 4.2 K. Cooling from 12 to 4.2 K causes a transfer of intensity from the central lines of the spectrum into the essentially fixed magnetic hyperfine lines rather than the Brillouin-like evolution of the hyperfine field, and hence line positions, that is characteristic of long-range magnetic ordering. The observed behavior is instead characteristic of the increasingly slow spin relaxation seen in spin-glass-like systems.

The low-temperature magnetic behavior of $Nd_{18}Li_5Co_4O_{39}$ is very different from that of $Nd_{18}Li_8Fe_5O_{39}$. The absence of hysteresis in $M(H)$ at high fields (Figure 8) and the frequency independence of $\chi(T)$ are both inconsistent with spin-glass-like behavior. It seems likely that the susceptibility maximum corresponds to a Néel point and that this compound is antiferromagnetically ordered below 2.3 K. Neutron diffraction data collected below 2 K are needed in order to confirm this hypothesis. The origin of the small hysteresis observed below 6 K in the magnetic susceptibility measured in a field of 100 Oe is not clear. One possible explanation is that spin clusters begin to form below this temperature. The hysteresis could then be caused by the restrictions imposed by crystalline anisotropy on the rotation of the net magnetic moment of the cluster. Cluster formation would also account for the nonlinearity of $M(H)$ at 4 K for $H > 20$ kOe, although nonlinearity might also be expected in a paramagnetic system for such large values of H/T.

Our original intention was to make new ferrimagnets by arranging two aliovalent magnetic cations on the octahedral 2*a* and 8*e* sites of the $La_{18}Li_8Rh_5O_{39}$ structure; on the basis of our experience with the rhodium-containing composition, we assumed that the prismatic 16*i* site would always be occupied by Li^+. In the case of $Nd_{18}Li_8Fe_5O_{39}$, we succeeded in ordering Fe^{4+} onto the 2*a* site, but 8*e*/16*i* site exchange between Fe^{3+} and Li^+ introduces disorder into the crystal structure. This disorder introduces frustration into the magnetic superexchange pathways and also introduces the possibility of direct exchange between cations in neighboring, face-sharing polyhedra. It may therefore be partly responsible for the failure of $Nd_{18}Li_8Fe_5O_{39}$ to achieve a magnetically ordered ground state. The complexity introduced when Fe^{3+} cations partially occupy the prismatic site mirrors that described above in the case of Ca_3NiMnO_6. Our original scheme envisaged only antiferromagnetic coupling along the individual polyhedral chains; we assumed that this would be stronger than any interchain coupling. However, the observation that the spins in the Nd−O framework freeze along with the iron spins shows that the interchain interactions in this material are too strong to be ignored. As a consequence of the 3-fold symmetry axis in the structure, these interactions introduce further frustration into the system.

Our planned investigation of the cobalt-containing analogue was disrupted somewhat by the formation of a metal-deficient composition. However, the negative temperature gradient of the susceptibility below T_N shows that the Nd^{3+} cations are also fully involved in the magnetic transition observed for this phase. The reduced transition temperature of $Nd_{18}Li_5Co_4O_{39}$, compared to that of $Nd_{18}Li_8Fe_5O_{39}$, probably reflects the partially filled nature of the transition-metal sublattice and the low magnetic moment of low-spin Co^{4+}. Indeed, the magnetic transition occurs at a sufficiently low temperature in $Nd_{18}Li_8Co_4O_{39}$ that it is reasonable to postulate that the interactions on the Nd^{3+} sublattices actually drive the ordering. The apparent formation by $Nd_{18}Li_5Co_4O_{39}$ of a long-range-ordered phase suggests that the lithium/iron site exchange is more responsible for the glassy behavior of $Nd_{18}Li_8Fe_5O_{39}$ than the frustration on the Nd^{3+} sublattices. However, this must be regarded as speculation until $Nd_{18}Li_5Co_4O_{39}$ has been studied by neutron diffraction at temperatures below 2 K.

Finally, we note that in view of the involvement of the Nd^{3+} sublattices in the magnetic transitions shown by these materials it is important, in order to understand the behavior of the transition-metal cations, to synthesize a phase in which these sublattices are occupied by diamagnetic cations.

Acknowledgment. The authors thank Dr. R. P. Hermann for many helpful and challenging discussions. S.E.D. thanks EPSRC and Somerville College, Oxford, U.K., for financial support. F.G. thanks the National Fund for Scientific Research, Belgium, for Grant 1.5.064.05. The authors are also grateful to ILL, Grenoble, France, for the provision of neutron facilities.

IC801529M